Small-Signal Stability Analysis of The Hydrokinetic Energy Harnessing connected to The Grid

W I Ibrahim[1], M R Mohamed[1] and R M T R Ismail[2]

[1]Sustainable Energy & Power Electronics Research Group (SuPER)
[2]Instrumentation & Control Engineering (ICE)
Faculty of Electrical & Electronics Engineering Technology
Universiti Malaysia Pahang,
26600 Pekan, Pahang, Malaysia

Abstract. This paper presents the modelling of the hydrokinetic system for the small-signal stability analysis under the small disturbances due to variation and fluctuation of water velocity in the river or marine. The complete modelling of the hydrokinetic system consists of vertical axis H-Darrieus turbine, direct-drive permanent magnet synchronous generator (PMSG), back-to-back converter and the grid network. By linearising all the equation around the steady-state value, the dynamic equation of the hydrokinetic system is derived. The stability of the system is tested with and without the PI controller. The eigenvalues analysis-based approaches have been used to investigate the stability of the system under the small disturbances. The findings show, the stability of the hydrokinetic system with PI controller is improved up to 57.82% by reducing the oscillation frequency at the Rotor Side Converter (RSC).

1. Introduction

The energy demand is growing significant nowadays due to the increase in the number population and enhanced living life worldwide [1]. Conversely, the depletion of fossil fuels, high CO_2 emission, global warming, and environmental pollution are the primary concern in the power generation field [2]. Therefore, Renewable Energy (RE) has the potential to play a significant role as a clean and sustainable energy resource for electricity generation in the future. The RE is reliable, key-climate solution and offers climate-safe energy by reduction of CO_2 emission and environmental friendly [3].

The hydrokinetic energy harnessing is one of the potentials energies in RE to provide the clean, sustain and reliable energy for the future generation. Hydrokinetics technology can be applied in the river, man-made channels, tidal and marine without the head or impoundment [4]. The concept of hydrokinetic is based on free-flowing stream that converts the kinetic energy of water velocity into electrical energy through the energy conversion scheme and power electronics converter.

Although the output capacity is small, however, the generation can be boosted by array or modular installation [5], [6]. In addition, the hydrokinetic system is based on free-flowing of water without the construction of the reservoir or impoundment [7]. Besides, the system is easy to transport and relocate due to the small size of the plant. Moreover, the system can be installed along the riverside, either mooring to fix structure or by floating pontoon [8].

Since the hydrokinetic is a new and emerging technology, several challenges and issues need to address, especially in controller strategies and analysis of small-signal stability. As the water velocity is fluctuation, the hydrokinetic system requires a sophisticated control strategy to extract output power and enhance efficiency. A few studies regarding hydrokinetic control system and strategies have been explored by past researchers using robust control [9]–[11] and pitch control strategies [12]–[14].

Small-signal analysis has been presented by many researchers in Wind Energy Conversion System (WECS) to design the controller or analyse the system stability in a grid network [15]–[19]. The state-space mathematical modelling of the wind turbine for the transient and small-signal analysis study in a weak network was derived in [20]. In addition, the stability analysis and grid-connected controller design based on diode bridge and boost converter were presented in [21].On the other hand, the analysis of the eigenvalues was used to study the small-signal analysis and the controller's parameter was designed based on traces of eigenvalues [22]. Furthermore, the analysis of the eigenvalues was also studied to evaluate the stability problem and improve the system stability under small disturbances [23], [24].

As far as authors concern, the literature regarding the small-signal analysis in the hydrokinetic system is scarce and limited. Nevertheless, the existing research on the small-signal analysis in WECS become the primary references. This is due to the concept, operation, and electrical hardware in the hydrokinetic system are resembles of WECS [25], [26]. In this paper, the mathematical model of the hydrokinetic system with direct-drive permanent magnet synchronous generator (PMSG) connected to the power network for small-signal analysis stability is presented. The full model of the hydrokinetic system consists of a water turbine, back-to-back converter, PMSG and grid network. In addition, the analysis of eigenvalues with and without a PI controller is presented to investigate the hydrokinetic system stability under small disturbances due to variation of the water.

2. Modelling of Hydrokinetic Energy Harnessing

Figure 1 illustrates the completed system of the hydrokinetic energy harnessing under studies. The system consists of the water turbine, PMSG, power electronics converter (PEC) and controller parts. The water turbine is immersed in the water and connected to the generator shaft through direct coupling without the gearbox system. The PMSG output is connected to the back-to-back converter to provide full access to active power control. The controller part comprises the Rotor Side Controller (RSC) and Grid Side Controller (GSC).

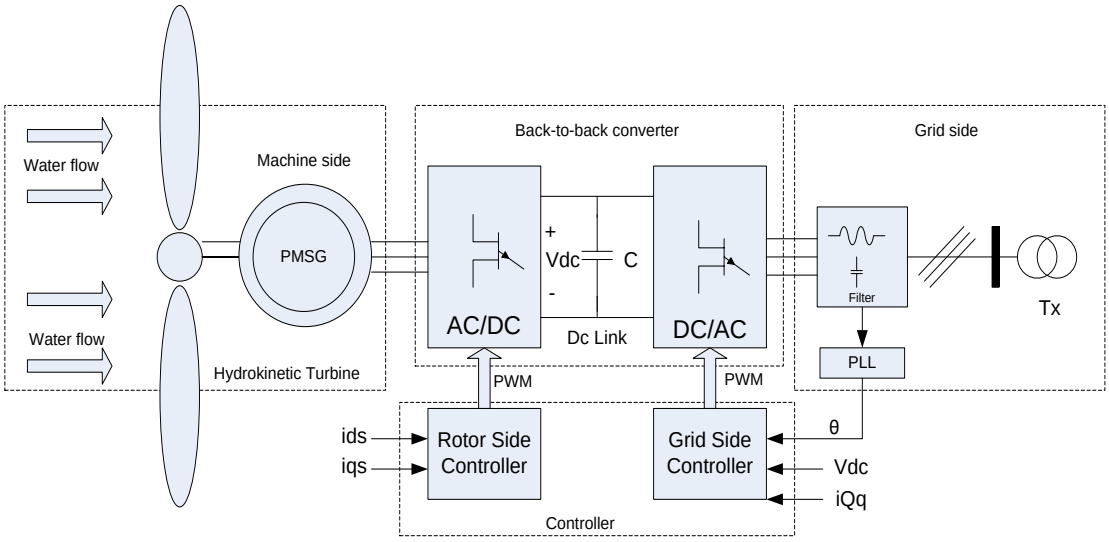

Figure 1. The hydrokinetic system in river energy harnessing

2.1. H-Darrieus Turbine Model

The turbine model is based on Vertical Axis straight blades H-Darrieus turbine. The design consideration of the turbine is discussed in [27] based on the river assessment studied at Pasir Kubur

River, Sungai Lembing, Kuantan, Pahang [28]. The mechanical torque of the turbine is given by Eq. (1).

$$T_m = \frac{0.5\rho A V^3 C_p}{\omega} \tag{1}$$

where, A is the area of the blade, ρ is the water density (1000 kg/m^3), C_p is the turbine power coefficient, V is the water velocity (ms^{-1}) and ω is the turbine's rotational speed. The C_p is represented as the power extraction efficiency at a different rotational speed of the turbine. It has a non-linear function of tip speed ratio (*TSR*) and the blade pitch angle, β. The turbine was operated at an optimal operating point at C_p=0.48 and TSR=2.4. Therefore, the C_p is given by Eq. (2).

$$C_P(\lambda) = -0.022\lambda^6 + 0.04\lambda^5 - 0.26\lambda^4 + 0.72\lambda^3 - 0.77\lambda^2 + 0.27\lambda - 0.011 \tag{2}$$

2.2. Modelling of PMSG

The PMSG with the constant magnetic flux, ψ_{pm} has been modelled in the *a-b-c* coordinates, *α-β* coordinates and as well as in the d-q reference frame. The conversion from a-b-c coordinates to d-q reference frame was related by the Clarke and Park transformation [29]. By aligning the direction of the d-axis of the d-q reference frame with the flux linkage (ψ_{pm}), the PMSG model is derived by Eq. (3) and (4) respectively.

$$V_{ds} = -R_s i_{ds} + \omega_e L_s i_{qs} - L_s \frac{di_{ds}}{dt} \tag{3}$$

$$V_{qs} = -R_s i_{qs} + \omega_e L_s i_{ds} - L_s \frac{di_{qs}}{dt} + \omega_e \psi_{pm} \tag{4}$$

where, V_{ds} and V_{qs} represented the stator voltage in d and q component respectively, i_{ds} and i_{qs} are the stator current in d and q component respectively, R_s and L_s are the resistance and inductance of the stator winding respectively, and ω_e is the generator electrical speed. Furthermore, the electromagnetic torque, T_e can be calculated by Eq. (5).

$$T_e = \frac{3}{2} n_p \psi_{pm} i_{qs} \tag{5}$$

where, n_p is the number of pole pairs. The Eq. (5) indicates that the T_e can be manipulated by controlling the q-axis current directly.

2.3. Drive Train Modelling

The water turbine and PMSG are connected directly without a gearbox. Hence, the mechanical system can be modelled using the one-mass model as given in Eq. (6).

$$\tau_j \frac{d\omega}{dt} = T_m - T_e \tag{6}$$

where, ω is the turbine speed, τ_j is the equivalent inertia time constant of the whole drive train. T_m and T_e are the mechanical and electromagnetic torque, respectively.

2.4. Model of The Converter

The H-Darrrieus turbine and PMSG are linked to the power grid system through back-to-back converters as shown in Figure 2. Therefore, the equation of power equilibrium can be written as given in Eq. (7).

$$P_{DC} = P_g - P_s \tag{7}$$

where, P_{DC} is the active power at the DC-Link, P_g and P_s are the active power at the grid and PMSG respectively. The details equations are given in Eq. (8)-(10).

$$P_{DC} = i_{DC} V_{DC} = C V_{DC} \frac{dV_{DC}}{dt} \tag{8}$$

where, V_{DC} is a capacitor terminal voltage, C is the capacitor and i_{DC} is the current of the capacitor.

$$P_g = V_{Dg} i_{Dg} + V_{Qg} i_{Qg} \tag{9}$$

where, V_{Dg} and $V_{Q}g$, are the d and q axis voltage at the GSC respectively, i_{Dg} and i_{Qg} are the d and q axis current of the GSC respectively.

$$P_s = V_{ds} i_{ds} + V_{qs} i_{qs} \tag{10}$$

where, V_{ds} and V_{qs} represented the stator voltage in d and q component respectively, i_{ds} and i_{qs} are the stator current in d and q component respectively. The model of the converter and DC-link can be derived as given in Eq. (11).

$$C V_{DC} \frac{dV_{DC}}{dt} = V_{Dg} i_{Dg} + V_{Qg} i_{Qg} - \left(V_{ds} i_{ds} + V_{qs} i_{qs} \right) \tag{11}$$

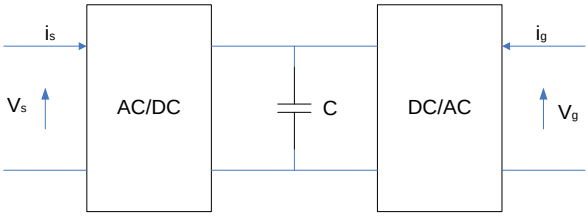

Figure 2. Back-to-back converter for modal analysis

2.5. Modelling of Power Grid

The grid network system can be modelled as follow;

$$V_g \angle \delta_g = V \angle 0 + j X_{TL} i_g \tag{12}$$

where, $V \angle 0$ is an infinite bus voltage, $V_g \angle \delta_g$ is a voltage at the grid and X_{TL} is a reactance of the transformer and transmission line. The modelling of power grid are given by Eq. (13) and (14) respectively.

$$i_{Dg} = \frac{V_{Dg} - V \sin \delta_g}{X_{TL}} \tag{13}$$

$$i_{Qg} = \frac{V_{Qg} - V \cos \delta_g}{X_{TL}} \tag{14}$$

3. The Controller Design

The function of the Rotor Side Controller (RSC) is to change the variable frequency AC power generated to DC voltage through the rectification process. Besides that, the RSC can gain maximum output power by controlling the generator rotational speed via the torque control method. This control method is achieved by controlling the quadrature current I_{qs}. On the other hand, the GSC is used to manage the DC-link voltage to keep constant and to convert the DC power to the grid AC power by

the inverter. The phase-locked loop (PLL) is used to match the frequency and phase of the grid-connected system.

3.1. Rotor Side Controller (RSC)

The stator current at direct-axis, i_{ds} is set to zero. The quadrature-axis stator current, i_{qs} is controlled to track the maximum output power from the fluctuation of the river current. The schematic diagram of RSC is shown in Figure. 3. The control equations of RSC are given by Eq. (15)- (21).

$$i_{ds}^{*} = 0 \tag{15}$$

$$\frac{dx_1}{dt} = i_{ds}^{*} - i_{ds} \tag{16}$$

$$V_{ds}^{*} = -K_{P1}\left(i_{ds}^{*} - i_{ds}\right) - K_{I1}x_1 + \omega_e L_s i_{qs} - R_s i_{ds} \tag{17}$$

$$i_{qs}^{*} = \frac{2T_e}{3n_p\psi_{pm}} \tag{18}$$

$$T_e = \frac{1}{2\lambda}\rho A R V^2 C_p \tag{19}$$

$$\frac{dx_2}{dt} = i_{qs}^{*} - i_{qs} \tag{20}$$

$$V_{qs} = -K_{P2}\left(i_{qs}^{*} - i_{qs}\right) - K_{I2}x_2 - \omega_e L_s i_{ds} - R_s i_{qs} \tag{21}$$

where, the intermediate state variables x_1 and x_2 are defined, K_P and K_I are the proportional and integral gains of the RSC, respectively.

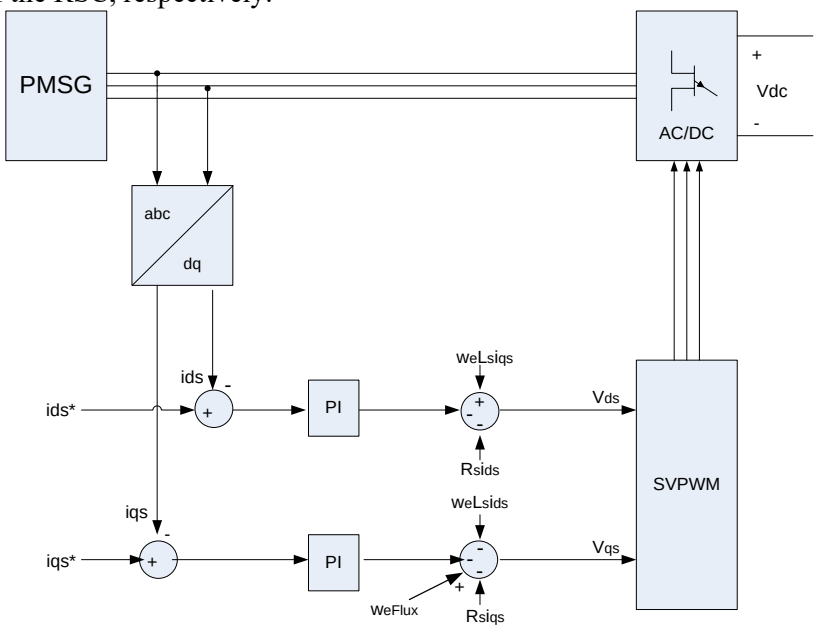

Figure 3. The schematic diagram of Rotor Side Controller (RSC)

3.2. Grid Side Controller (GSC)

By aligning the vector voltage, V_g to the direction of Q-axis, the V_{Dg} is equal to zero and the active power $P_g = V_{Qg} i_{Qg}$. The model of GSC are given by Eq. (22) and (23).

$$L\frac{di_{Dg}}{dt} = V_{Dg} - V_{Dm} + \omega L i_{Qg} \tag{22}$$

$$L\frac{di_{Qg}}{dt} = V_{Qg} - V_{Qm} + \omega L i_{Dg} \tag{23}$$

The direct-axis of grid current is set to zero, (i_{Dg} =0) to obtain the reactive power at the grid equal to zero, (Q_G=0). Hence, the DC voltage can be preserved by controlling the quadrature-axis grid current, i_{Qg}. The control equation for GSC are given by Eq. (24)-(30).

$$i_{Dg}{}^{*} = 0 \tag{24}$$

$$\frac{dx_3}{dt} = i_{Dg}{}^{*} - i_{Dg} \tag{25}$$

$$V_{Dm}{}^{*} = -K_{P3}\left(i_{Dg}{}^{*} - i_{Dg}\right) - K_{I3}x_3 + \omega L i_{Qg} - V_{Dg} \tag{26}$$

$$\frac{dx_4}{dt} = V_{DC}{}^{*} - V_{DC} \tag{27}$$

$$i_{Qg}{}^{*} = K_{P4}\left(V_{DC}{}^{*} - V_{DC}\right) + K_{I4}x_4 \tag{28}$$

$$\frac{dx_5}{dt} = i_{Qg}{}^{*} - i_{Qg} \tag{29}$$

$$V_{Qm} = -K_{P5}\left(i_{Qg}{}^{*} - i_{Qg}\right) - K_{I5}x5 - \omega L i_{Dg} + V_{Qg} \tag{30}$$

where, the intermediate state variable are represented by x_3, x_4, x_5 and x_6 , i_{Dg} and i_{Qg} are the direct-quadrature axis grid current respectively, V_{Dg} and V_{Qg} are the *d-q* axis grid voltages, V_{DC} is the DC-link voltage, K_P and K_I are the proportional and integral controller constants respectively. The schematic diagram of GSC as shown in Figure 4.

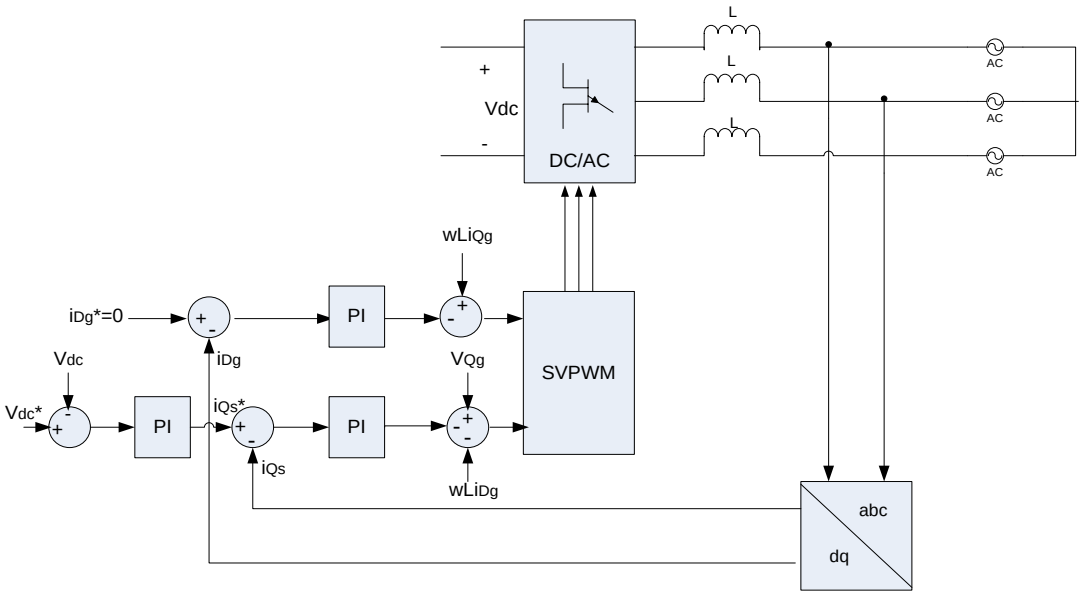

Figure 4. The schematic diagram of the Grid Side Controller (GSC)

4. Small-signal Stability Analysis

The dynamic model of the completed hydrokinetic system has been linearised around the steady-state value for the small-signal stability analysis. The lists of the equation are represented as follow, Equation (3)-(4) is described the model of the PMSG, whereas Equation (5) for the dynamic model of the turbine. The DC-link model is represented by Equation (11), whereas Equation (15)-(21) and Equation (24)-(30) are represented the dynamic model of the controller design at RSC and GSC respectively. Lastly, the dynamic model of the electric grid system is given by Equation (22)-(23). The whole equations can be represented by the state-space equation as given in Eq. (31).

$$\frac{d\Delta x}{dt} = A\Delta x + B\Delta u \tag{31}$$

where, A is the $[11\times11]$ state matrix, B is the $[1\times11]$ state matrix, Δx is a vector of state variables, and Δu is a vector state variable of the input as given in Eq. (32) and (33) respectively.

$$x = \left[\, \omega \;\; i_{ds} \;\; i_{qs} \;\; x_1 \;\; x_2 \;\; x_3 \;\; x_4 \;\; x_5 \;\; i_{Dg} \;\; i_{Qg} \;\; V_{DC} \,\right]^T \tag{32}$$

$$u = V_w \tag{33}$$

5. Results and Discussions

The small-signal analysis of the hydrokinetic system with direct-drive PMSG connected to the grid network is analysed using the Matlab software. The turbine, PMSG and controller parameter under studies are given at appendices. In this case, the analysis of eigenvalues has been applied to evaluate the system stability under small disturbances. For the first stage of analysis, the system without the PI controller is investigated. The system consists of 4th order to represent the four states which are $x = \left[\, \omega \;\; i_{ds} \;\; i_{qs} \;\; V_{DC} \,\right]^T$.

Table 1 shows the eigenvalues of the 4th order model without the PI controller. As can be seen in Table 1, the state λ_4 is represented the V_{DC} is at the unstable condition. This is due to the poles is at the right of the region which is a positive real part. In addition, the states $\lambda_{2,3}$ which represented the i_{ds} and i_{qs} respectively are conjugated roots with large imaginary parts. As noted in [22], the larger imaginary part will produce the large oscillation frequency in the system due to the disturbances. Therefore, the hydrokinetic system without the PI controller can be concluded as an unstable system, even the states λ_1 and $\lambda_{2,3}$ at the left plane region.

Table 1. The Eigenvalues of State Matrix A without PI controller

State	Eigenvalues	Oscillation Frequency (Hz)	Damping Ratio
λ_1	-8.14	0	1
λ_2	-106.36 + 89.53i	14.25	0.765
λ_3	-106.36 - 89.53i	14.25	0.765
λ_4	945.65	0	1

In the second stage, the PI controller is added to investigate the impact on system stability. The 11th order model was derived as given in Equation (32). Table 2 shows the eigenvalues, oscillation frequency and damping ratio of 11th order model with PI controller. As can be seen, all the eigenvalues have a negative real part. The stator current (i_{ds} and i_{qs}) and DC-link voltage show high oscillation frequency. It is observed that, all the eigenvalues have a negative real part; hence, proves that the system is in a stable condition even after suffering small disturbance. The system consists of three evanescent modes for states λ_1, λ_6 and λ_7, whereas, four states are listed in oscillation modes as follows, $\lambda_{2,3}$, $\lambda_{4,5}$, $\lambda_{8,9}$ and $\lambda_{10,11}$.

Table 2. The eigenvalues of state Matrix A with PI Controller

No.	Eigenvalues	Oscillation Frequency, (Hz)	Damping ratio
λ_1	-8.14	0	1
$\lambda_{2,3}$	-53.18 ±37.77i	6.01	0.815
$\lambda_{4,5}$	-106.36±99.80i	15.88	0.73
λ_6	-278.65	0	1
λ_7	-46.70	0	1
$\lambda_{8,9}$	-21.40±4.74i	0.754	0.976
$\lambda_{10,11}$	-492.47±204.30i	32.51	0.923

The spectrum analysis of Matrix A is shown in Figure 5. As can be seen, all the states are at the left of the region. Therefore, it is proved, with the PI controller, the stability of the hydrokinetic system can be enhanced. The oscillation frequency at the state $\lambda_{2,3}$ for example, is reduced to 6.01 Hz compared to 14.25 Hz without the PI controller. The finding shows that the PI controller able to suppress the oscillation of generator stator current (i_{ds} and i_{qs}) at the RSC up to 57.82% under small

disturbance. Furthermore, system stability is improved when all the states maintain in the left region of the plane.

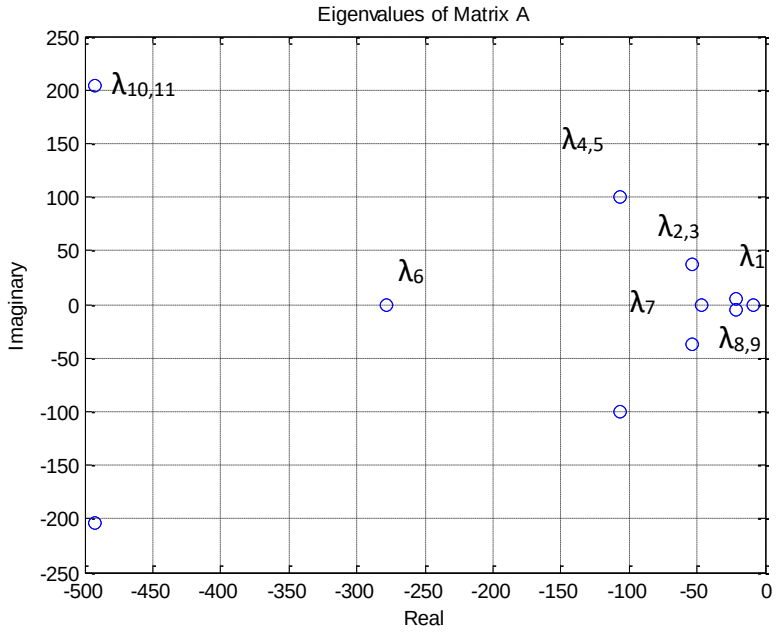

Figure. 5. The spectrum analysis of Matrix A

6. Conclusion

This paper presents the small-signal stability analysis of the hydrokinetic system under small disturbances of water velocity. In this study, the finding shows the hydrokinetic system is unstable without the PI controller due to the state λ_4 is placed on the right region. Nevertheless, the PI controller has improved the system stability, and all the states are in the left region. In addition, the analysis of the eigenvalues has improved the stability of the system by reducing the oscillation frequency up to 57.82% of the generator stator current (i_{ds} and I_{qs}) at the RSC.

7. Appendices

Appendix A: The parameter of H-Darrieus Turbine

Water density, ρ = 1000 kg/m^3; *Radius* = 0.5 m; *Height* = 0.8 m; C_P optimal = 0.48; *TSR* = 2.54;

Appendix B: The parameter of PMSG

n_p =28; R_s = 1.74 Ω; L_S = 36.2 mH; Ψ_{pm} = 2.32 Wb.

Appendix C: The parameter of PI controller

K_{P1} = *0.5 pu;* K_{I1}*=20/s;* K_{P2} = *1 pu;* K_{I2} = *100/s;* K_{P3} *0.5 pu;* K_{I3} *=20;* K_{P4} = *0.4 pu;* K_{I4} = *20/s;* K_{P5} *=0.5 pu;* K_{I5}*=20/s*

Appendix D: Matrix A $[11\times11]$

$$A = \begin{pmatrix} a_{11} & 0 & a_{13} & 0 & 0 & 0 & 0 & 0 & 0 & 0 & 0 \\ 0 & a_{22} & 0 & a_{24} & 0 & 0 & 0 & 0 & 0 & 0 & 0 \\ 0 & 0 & a_{33} & 0 & a_{35} & 0 & 0 & 0 & 0 & 0 & 0 \\ 0 & a_{42} & 0 & 0 & 0 & 0 & 0 & 0 & 0 & 0 & 0 \\ 0 & 0 & a_{53} & 0 & 0 & 0 & 0 & 0 & 0 & 0 & 0 \\ 0 & 0 & 0 & 0 & 0 & 0 & 0 & 0 & a_{69} & 0 & 0 \\ 0 & 0 & 0 & 0 & 0 & 0 & 0 & 0 & 0 & 0 & a_{711} \\ 0 & 0 & 0 & 0 & 0 & 0 & a_{87} & 0 & 0 & a_{810} & a_{811} \\ 0 & 0 & 0 & 0 & 0 & a_{96} & 0 & 0 & a_{99} & 0 & 0 \\ 0 & 0 & 0 & 0 & 0 & 0 & a_{107} & a_{108} & 0 & a_{1010} & a_{1011} \\ a_{111} & a_{112} & a_{113} & a_{114} & a_{115} & 0 & 0 & 0 & a_{119} & a_{1110} & a_{1111} \end{pmatrix}$$

8. References

[1] D. C. Baruah and C. C. Enweremadu, "Prospects of decentralized renewable energy to improve energy access: A resource-inventory-based analysis of South Africa," *Renew. Sustain. Energy Rev.*, vol. 103, no. 3, pp. 328–341, 2019.

[2] M. Kaltschmitt and D. Thrän, "Bioenergy," in *Managing Global Warming. An Interface of Technology and Human Issues*, Academic Press, 2019, pp. 346–351.

[3] F. La Camera, "People , Planet and Prosperity. Raising Climate Ambitions Through Renewables.," *International Renewable Energy Agency*, pp. 1–24, 2019.

[4] M. I. Yuce and A. Muratoglu, "Hydrokinetic energy conversion systems: A technology status review," *Renew. Sustain. Energy Rev.*, vol. 43, pp. 72–82, 2015.

[5] E. Alvarez Alvarez, M. Rico-Secades, E. L. Corominas, N. Huerta-Medina, and J. Soler Guitart, "Design and control strategies for a modular hydroKinetic smart grid," *Int. J. Electr. Power Energy Syst.*, vol. 95, pp. 137–145, 2018.

[6] M. A. R. Shafei, D. K. Ibrahim, A. M. Ali, M. A. A. Younes, and E. E. D. A. El-Zahab, "Novel approach for hydrokinetic turbine applications," *Energy Sustain. Dev.*, vol. 27, no. 2015, pp. 120–126, 2015.

[7] L. I. Lago, F. L. Ponta, and L. Chen, "Advances and trends in hydrokinetic turbine systems," *Energy Sustain. Dev.*, vol. 14, no. 4, pp. 287–296, 2010.

[8] M. Anyi and B. Kirke, "Evaluation of small axial flow hydrokinetic turbines for remote communities," *Energy Sustain. Dev.*, vol. 14, no. 2, pp. 110–116, 2010.

[9] B. Eddine, Seif Elghali, H. El, Mohamed Benbouzid, T. Ahmed-ali, and J. F. Charpentier, "High-Order Sliding Mode Control of a Marine Current Turbine Driven Doubly-Fed Induction Generator," *IEEE J. Ocean. Eng.*, vol. 35, no. 2, pp. 402–411, 2010.

[10] V. J. Ginter and J. K. Pieper, "Robust gain scheduled control of a hydrokinetic turbine," *IEEE Trans. Control Syst. Technol.*, vol. 19, no. 4, pp. 805–817, 2011.

[11] K. Jahangir, I. Tariq, and J. Quaicoe, "Evaluation of maximum power point tracking in hydrokinetic energy conversion systems," *J. Eng.*, no. 11, pp. 331–338, 2015.

[12] K. Takagi, Y. Suyama, and K. Kagaya, "An attempt to control the motion of floating current turbine by the pitch control," in *2011 IEEE OCEANS*, 2011, pp. 1–6.

[13] X. Xue, "Development of A NonLinear wind Turbine Simulator for Linear Parameter-Varying Control Design," China University of Mining & Technology Beijing, 2015.

[14] Z. Xue-wei, W. Shu-qi, W. Feng, Z. Liang, and S. Qi-hu, "The Hydrodynamic Characteristics of Free variable-Pitch Vertical Axis Tidal Turbine," *J. Hydrodyn.*, vol. 24, no. 6, pp. 834–839, 2012.

[15] T. Knüppel, J. N. Nielsen, K. H. Jensen, A. Dixon, and J. Ostergaard, "Small-signal stability of

wind power system with full-load converter interfaced wind turbines," *IET Renew. Power Gener.*, vol. 6, no. 2, p. 79, 2012.
[16] J. Hu, B. Wang, W. Wang, H. Tang, Y. Chi, and Q. Hu, "Small Signal Dynamics of DFIG-Based Wind Turbines during Riding Through Symmetrical Faults in Weak AC Grid," *IEEE Trans. Energy Convers.*, vol. 32, no. 2, pp. 720–730, 2017.
[17] J. Hu, Y. Huang, D. Wang, H. Yuan, and X. Yuan, "Modeling of Grid-Connected DFIG-Based Wind Turbines for DC-Link Voltage Stability Analysis," *IEEE Trans. Sustain. Energy*, vol. 6, no. 4, pp. 1325–1336, 2015.
[18] Z. Wei *et al.*, "Probabilistic Small Signal Stability Analysis of Power System with Large Scale Wind Power," in *IEEE Transportation Electrification Conference and Expo (ITEC Asia-Pacific 2014)*, 2014, pp. 1–4.
[19] M. F. M. Arani and Y. A. R. I. Mohamed, "Analysis and Impacts of Implementing Droop Control in DFIG-Based Wind Turbines on Microgrid/Weak-Grid Stability," *IEEE Trans. Power Syst.*, vol. 30, no. 1, pp. 385–396, 2015.
[20] C. E. Ugalde-loo, J. B. Ekanayake, S. Member, and N. Jenkins, "State-Space Modeling of Wind Turbine Generators for Power System Studies," *IEEE Trans. Ind. Appl.*, vol. 49, no. 1, pp. 223–232, 2013.
[21] M. Rahimi, "Drive train dynamics assessment and speed controller design in variable speed wind turbines," *Renew. Energy*, vol. 89, pp. 716–729, 2016.
[22] H. H. C. Mao and J. L. D. Wang, "Small-signal modelling and analysis of wind turbine with direct drive permanent magnet synchronous generator connected to power grid," *IET Renew. Power Gener.*, vol. 6, no. 1, pp. 48–58, 2012.
[23] J. S. Kani, S. G. B. Dasan, S. Ravichandran, and R. P. K. Devi, "Small signal stability analysis of PMSG based WECS with coordinated controller tuning," in *Proceeding of the 2014 IEEE International Conference on Green Computing, Communication and Electrical Engineering*, 2014, pp. 1–6.
[24] M. Chouket and L. Krichen, "Small Signal Modeling and Stability Analysis of Wind Turbine with PMSG Connected to The Grid," in *2015 IEEE 12th International Multi-Conference on Systems, Signals and Devices*, 2015, vol. 2, pp. 1–8.
[25] S. P. Koko, K. Kusakana, and H. J. Vermaak, "Optimal energy management of a grid-connected micro-hydrokinetic with pumped hydro storage system," *J. Energy Storage*, vol. 14, pp. 8–15, 2017.
[26] H. Chen, T. Tang, N. Ait-Ahmed, M. E. H. Benbouzid, M. MacHmoum, and M. E. H. Zaim, "Attraction, Challenge and Current Status of Marine Current Energy," *IEEE Access*, vol. 6, pp. 12665–12685, 2018.
[27] W. I. Ibrahim, R. M. T. R. Ismail, and M. R. Mohamed, "Hydrokinetic Energy Harnessing for River Application," *J. Telecommun. Electron. Comput. Eng.*, vol. 10, no. 1, pp. 133–138, 2018.
[28] W. I. Ibrahim, R. M. T. R. Ismail, and M. R. Mohamed, "Micro-Hydro Energy Estimation for Hydrokinetic Energy Harnessing at Sungai Lembing," in *Proceedings of the 10th National Technical Seminar on Underwater System Technology (Nusys 2018)*, 2019, vol. 538.
[29] B. Ren, Y. Wang, and Q. C. Zhong, "UDE-based control of variable-speed wind turbine systems," *Int. J. Control*, vol. 90, no. 1, pp. 121–136, 2017.

Acknowledgments
The authors would like to thank to Universiti Malaysia Pahang for funding support under UMP Postgraduate Research Scheme (PGRS190318).